ISSN:1687-1006

The Egyptian International Journal of Engineering Sciences and Technology

Vol. 30 (2020) 22–38

https://eijest.journals.ekb.eg/

Experimental study for the performance of an integrated solar collector water heater based on helical fins heat pipes using phase changing material

Mohamed A. Ahmed[a], Ibrahim Y. Rofaiel[a*], Mohamed A. Essa[a,b]

[a]*Department of mechanical power engineering, faculty of engineering, Zagazig University, 44519 Zagazig, Egypt.*
[b] *Mechanical Department, College of Engineering, Shaqra University, Dawadmi, 11911 Saudi Arabia.*

ARTICLE INFO

Keywords:

Evacuated tube solar collector
Phase change materials
Paraffin
Thermal storage
Helical finned heat pipes.

ABSTRACT

One of the most promising solar heaters is the evacuated tube solar collector (ETSC). Enhancing the performance of ETSCs using latent heat energy storage system has been widely investigated. Accordingly, paraffin wax as phase changing material (PCM) has taken a large portion of research work. Although paraffin wax has a significant disadvantage of having low thermal conductivity, using fins to enhance the overall heat transfer coefficient has been studied to overcome such drawback. The present work compares experimentally the performance of two evacuated tubes systems having two novel fins systems. Namely; an ETSC with copper helical fins of 20 mm pitch and an ETSC with copper helical fins of 40 mm pitch. The experimental work was done under four different flow rates to investigate the effect of the thermal load on the systems performance. These flow rates are; 0.165 L/min, 0.335 L/min, 0.5 L/min and 0.665 L/min with normal water as the heat transfer fluid (HTF). In addition, the PCM temperature inside the evacuated tubes are measured along the tube axis to investigate the fins effect on PCM temperature homogeneity and thermal storage. The systems performances and daily efficiencies are also compared to emphasis the effect of fins configurations. The experimental results have shown that both systems provided a proper PCM temperature homogeneity ant peak temperatures. However, both systems have shown different trends for PCM temperature distribution along the tubes axis. A peak HTF temperature of 53 ˚C was achieved in the system with 40 mm helical pitch fins. Both systems have successfully supplied hot HTF throughout the night for the four different flow rates. However, regarding daily efficiency, the 20 mm pitch system provide an enhancement of 11.85% with maximum efficiency of 68.66% at 0.665 L/min flow rate.

1. Introduction

In recent years, Earth has seen a global trend to be more dependent on renewable energy sources. This is to make up for the continuously depleting non-renewable energy sources. Solar energy has been given the most interest in the field of renewable energy. This is because of the massive amounts of solar radiation that Earth receives on daily basis. However, as solar energy is only available during the day, an energy storage system is needed to deliver energy through the night. Although many storage systems are currently available, phase changing materials (PCM) still remain the most promising. PCMs have the advantage of storing thermal energy

* Corresponding author. Tel. 00201223038166.
E-mail address: ibrahim-rofaiel@hotmail.com

in the form of latent energy. When solar radiation becomes scarce, the stored energy can be transferred to the HTF at an almost constant temperature during phase change. Moreover, PCMs are generally compact when compared to sensible heat storage systems. One of the main classifications of PCMs is according to the melting temperature. Although PCMs can be used with different types of solar collectors such as flat plate collectors (FPCs), they are better suited for ETSCs because the vacuum layer between the two concentric tubes of the evacuated tube act as a thermal insulation which ensures the occurrence of PCM phase change with minimal solar radiation. Accordingly, the subject of PCM integrated ETSCs has been studied by researchers as a viable solar collector system for around the day use. S.D. Sharma et al. [1] performed and experimental study to investigate the performance of a solar cooker using PCM integrated ETSC. Erythritol was used as the PCM. The study aimed to investigate whether the system was able to be utilized for both evening and noon cooking. The study concluded that the system was a viable option for community usage where the PCM temperature was kept at an elevated level of almost 75 ˚C until the next morning. However, the author highlights the system high initial cost. M.S. Naghavi et al. [2] studied theoretically a model for a PCM integrated solar water heater composed of an evacuated tube collector with a PCM integrated manifold. Paraffin wax was considered as the PCM while tap water was considered as the HTF. The PCM integrated system was compared to a conventional system without PCM through both charging and discharging cycles. The study concluded that the PCM system performance was better than that without PCM at flowrates higher than 55 L/h. It was also found that the PCM system performance was less affected by changing the HTF flowrate. Neeraj Mehla et al. [3] investigated experimentally the thermal performance of an ESTC solar air heater integrated with Acetamide as PCM. The heat transfer process between PCM and air was enhanced using two different fins systems, namely; copper coil and circular fins. The proposed fins systems had an enhancing effect on the systems efficiencies. A maximum temperature difference between heated and cool air of 37 ˚C and 20.2 ˚C for sunshine hours and off-sunshine hours was achieved using circular fins. The same author [4] conducted further study to investigate the performance of the same Acetamide integrated ETSC solar air heated during simultaneous and consecutive charging and discharging cycles under a wide range of HTF flowrate. The experimental results showed that for high flowrates, the maximum efficiency was achieved during the simultaneous charging and discharging performance and was equal 17.9%. The consecutive charging and discharging system achieved an efficiency of 11.89% for the same flow rate. A desiccant dehumidifier was also investigated by Neeraj Mehla et al. [5]. The dehumidifier also utilized ETSC coupled with Acetamide PCM. Different flow rates performance was investigated. The study concluded that using PCM allowed the system to work continuously for 14 hours. This was considered a major enhancement for the system performance. Yaxiong Wang et al. [6] investigated experimentally the performance of a solar air heater consisting of finned heat pipes evacuated tubes integrated with modified paraffin wax. The system performance considered different flowrates, elevation angles, ambient temperature and radiation intensity. Under the tests conditions, the optimum elevation angle was found to be 60˚. The system performance was found to be enhanced under high flow rates. A maximum heat dissipation efficiency of 97% was achieved for the system. Sheng Xue [7] compared experimentally the performance of two solar water heaters, namely; conventional water in glass ETSC and U-tube ETSC heater integrated with Barium hydroxide as PCM. Two modes of operation were investigated; exposure and constant flow modes. Under exposure conditions, the PCM integrated system performance was inferior to that of water in glass system. The author explained this by the high viscosity and low thermal conductivity of the PCM. On the other hand, under constant flow rate conditions, the PCM integrated system provided a higher system efficiency by almost 20%. Mohamed A. Essa et al. [8] experimentally investigated the effect of the phase change process on the system performance of a U-tube ETSC integrated with paraffin wax under different flow rates. The PCM integrated system was compared to a control system without PCM. A novel fin system was utilized with the PCM system. An empirical formula was also presented relating the discharge time to the discharge temperature. The study showed that maximum performance enhancement of 21.9% was achieved by the PCM system under low flow rates where full phase change occurred. Higher flowrates hindered the process of phase change which caused the PCM to have no energy storage effect. However, the PCM system daily efficiency was still higher than that of the control system. At medium flow rates were partial phase change occurred, the PCM showed some energy storage effect but showed system daily deterioration of 12% compared to the control collector. Abokersh et al. [9] experimentally investigated the performance of solar water heaters

based on U-tube ETSC integrated with paraffin wax. Three configurations were studied, namely; ETSC without PCM, ETSC with PCM and ETSC with PCM and novel fins systems denoted A, B and C, respectively. Systems B and C showed performance enhancement over system A. The annual efficiency for systems A, B and C were 40.5%, 71.8% and 85.7%, respectively under constant flow conditions. On the other hand, the systems annual efficiency was 20%, 33% and 26% for systems A, B and C, respectively under real consumption profiles. R. Sekret et al. [10] compared experimentally the performance of conventional heat pipe ETSC system to that of paraffin integrated heat pipe ETSC system for heating water. Results showed that PCM integration prolonged the period of obtaining useful thermal energy and hot water. However, the peak HTF temperature for the conventional system was higher than that of the PCM integrated system because a portion of the collected energy is transferred and stored within the PCM. It is noted that the lower HTF temperature was considered as an advantage because the excessive heating would cause greater thermal losses. Results also showed that the PCM integration raised the amount of useful energy delivered by the system by 45-79%. Piotr Feliński et al. [11] studied experimentally the effect of integrating hydrotreated paraffin wax into an ETSC water heater. The study showed that during peak loads, PCM integration prolonged the process of heat release. The PCM integrated system has an enhancement of the annual solar fraction by 20.5%. However, it is noted that neither system was able to provide hot water during cold seasons. The same author [12] also experimentally investigated the enhancing effects of incorporating a PCM integrated ETSC water heated with a compound parabolic concentrator (CPC). Paraffin wax was also used as the PCM. The CPC incorporated system has shown an enhancement for the charging efficiency from 31% to 36%. CPC incorporation also raised the maximum efficiency from 40% to 49%. Papadimitratos et al. [13] investigated experimentally the performance of a PCM integrated ETSC and conventional ETSC under both stagnation and normal operation. Both systems had ten evacuated tubes. The PCM integrated system showed an efficiency increase of 26% and 66% under normal and stagnation operation respectively. M.S. Naghavi et al. [14] investigated experimentally the performance of a PCM integrated solar water heater. The system utilized heat pipes evacuated tubes with finned condensers. The PCM was integrated inside a storage tan where the heat pipes condensers were fitted. During sunny days, the system had efficiency in the range of 38%-42%. However, the system efficiency was slightly decreased to the range of 34%-36% during cloudy days. Fatemeh Hassanipour et al. [15] experimentally investigated utilizing Carbon Nanotubes (CNT) sheets to enhance evacuated tubes solar absorption. The study also considered integrating Octadecane paraffin PCM as latent heat storage system. Results showed that the CNT sheets presented a near black body performance absorbing almost 98% of solar radiation. Results also showed that integrating the PCM with the CNT sheets prolonged the period of energy dissipation even during cloudy days. A temperature of 50˚ was achieved by using 15 layers of CNT and 14 grams of PCM on cloudy days. Xiaoqiang Zhai et al. [16] investigated both theoretically and experimentally the performance of an ETSC water heater integrated with composite PCM. Four different PCMs were considered, namely; Erythritol with 1%, 2%, 3% and 4% wt expanded graphite. The evacuated tubes utilized heat pipes and PCM was placed inside the evacuated tubes within aluminum pipes. Based on the results, the 3% wt expanded graphite PCM was chosen as the proper composite PCM. The study found that the storage efficiency peaked at 40.17% for mid-temperature applications. The same author [17] also conducted further studies on the composite PCM integrated ETSC water heater. The 3% wt expanded graphite was utilized as the PCM. The evacuated tubes had some modifications. Different flowrates and different water inlet temperatures were also considered. Results showed that the daily storage efficiency reached 39.98% during a sunny day. P. Manoj Kumar et al. [18] experimentally investigated the performance of three solar water heating systems based on water in glass ETSC. The three systems were namely, one without PCM, the second wit paraffin wax PCM and the third with nano-composited paraffin wax PCM (NCPCM). The NCPCM was composed of paraffin wax and SiO2 nano particles. The nano particles are noted to improve the poor thermal conductivity of the paraffin wax. Both the PCM and NCPCM systems provided an improved performance compared to the system without PCM. Where, the no-PCM, PCM and NCPCM systems had efficiencies of 58.74%, 69.62% and 74.79%, respectively.

The previous literature shows that PCM integration with ETSCs provides possible performance enhancements including: prolonging the time of useful energy dissipation, increasing system efficiency and minimizing the gap between demand and supply. However, PCMs such as paraffin wax are faced with the limitation of low thermal conductivity

which may hinder energy transfer to the HTF. Thus, great interest is given to raising the PCM thermal conductivity by utilizing and efficient fins system. The present work investigates the performance of PCM integrated heat pipes ETSCs utilizing two novel helical fins systems with different pitches. The study also investigates the effect of HTF flowrate on systems performance as well as energy storage within the PCM. The study considers the two systems simultaneously to further emphasis the performance comparison.

2. Experimental setup

The present work experimentally investigates the performance of PCM integrated finned heat pipe ETSC. Two collectors are considered simultaneously. The first utilizes novel helical fins of 20 mm pitch (Collector A) while the other utilizes novel helical fins of 40 mm pitch. The experimental test rig was set up on the roof top of Mechanical power engineering department, Zagazig University (Longitude=31.5041°E, Latitude=30.5765 °N), Egypt. Both collectors are facing south and tilted at an angle of 35˚ based on the site latitude. Paraffin wax is used as the PCM and is integrated inside the evacuated tubes. Each collector consisted of 5 evacuated tubes of 1.8 m length and 58 mm external diameter with total aperture area of 0.47 m^2. Finned heat pipes are placed inside the evacuated tubes. Each collector has a common manifold where the heat pipes condensers are inserted. Water which is considered the HTF passes through the manifold gaining heat from the heat pipes condensers as shown in Figure 1.

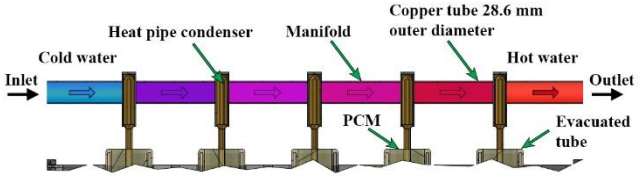

Figure 1. Manifold principle of operation

Water is circulated via a 0.5 HP pump from a 1000 L open top tank through the collectors and back to the tank. Therefore, the tank represents the thermal load, where its large volume and open top ensures that the water inlet temperature to the collectors is not affected with the heating process. Flow control valves and a bypass valve are used to accurately control the HTF flow rates flowing through each collector. A schematic diagram of the system is shown in Figure 2, while a picture of the experimental test rig is shown in Figure 3. Each tube is filled with commercial grade paraffin wax. The detailed properties of the commercial paraffin wax are presented in Table 1.

Table 1 Paraffin wax physical properties

Melting temperature	58-65, ˚C
Solid phase density	0.92, kg/m3
Liquid phase density	0.79, kg/m3
Specific heat	2.3, kJ/kg.K
Latent heat of fusion	189, kJ/kg
Thermal conductivity	0.21, W/m.K

The proposed helical fins systems are manufactured by cutting single circular copper disks of 0.5 mm thickness using a cutting mold. The disks are then pressed into a single helical pitch with a 42 mm and 8 mm outer and inner diameters respectively. These single pressed disks are then soldered together and point welded to the heat pipes to ensure proper contact. Two systems are considered, the first (System A) has a 20 mm helical pitch and the other (System B) has a 40 mm helical pitch as shown in Figure 4. The smaller pitch means that system A has a larger fins surface area.

It's worth noting that the traditional fins usually used with heat pipes have a small thickness and weak construction. Thus, they almost always have some deformation. This makes it very difficult to maintain good contact with the heat pipe and the evacuated tube wall along its length. This presents a major advantage for the proposed fins systems which allows for better contact along the length of the evacuated tube and heat pipe. This provides better heat transfer to the PCM and consequently better collector's performance.

2.1. Measurements

The experimental tests were carried out at four flowrates, namely; 0.165, L/min, 0.355, L/min, 0.5, L/min and 0.665, L/min. The HTF flowrate was measured for each collector by two independent flowmeters in series to ensure the results accuracy. The first is a visual Dahror DFG-10 acrylic rotameter with an accuracy of ± 4%. The second is an analog

micro flowmeter of type Saier SEN-HZ06S with accuracy ranging from 5% to 8%. Moreover, the PCM temperature inside a reference tube in each collector is recorded using K-type thermocouples of ± 2.2 ˚C accuracy. In each collector, four thermocouples placed at equal four spacing along the reference tube axis, in order to detect the fins effects on PCM temperature distribution and homogeneity in both charging and discharging cycles. The HTF inlet and outlet temperatures for both collectors are measured using waterproof LM35 thermistor of ± 0.5, ˚C accuracy. To evaluate the systems daily efficiencies, global and diffused solar radiations were recorded every ten minutes using a solar power meter of type PYR-1307 and ± 10 W/m2 accuracy. Ambient conditions, namely; ambient temperature and wind speed were recorded using Pasco Xplorer GLX PS-2002 data logger. The logger is coupled with a rotary motion sensor type PS-2120A and a weather anemometer sensor module PS-2174 of ± 3% and ± 0.5, ˚C accuracy, respectively. Readings from the water proof thermistors, micro flowmeters and K-type thermocouples were recorded and logged using a Mega 2560 microcontroller Arduino board. The board was also fitted with eight MAX6675 modules to incorporate the eight thermocouples.

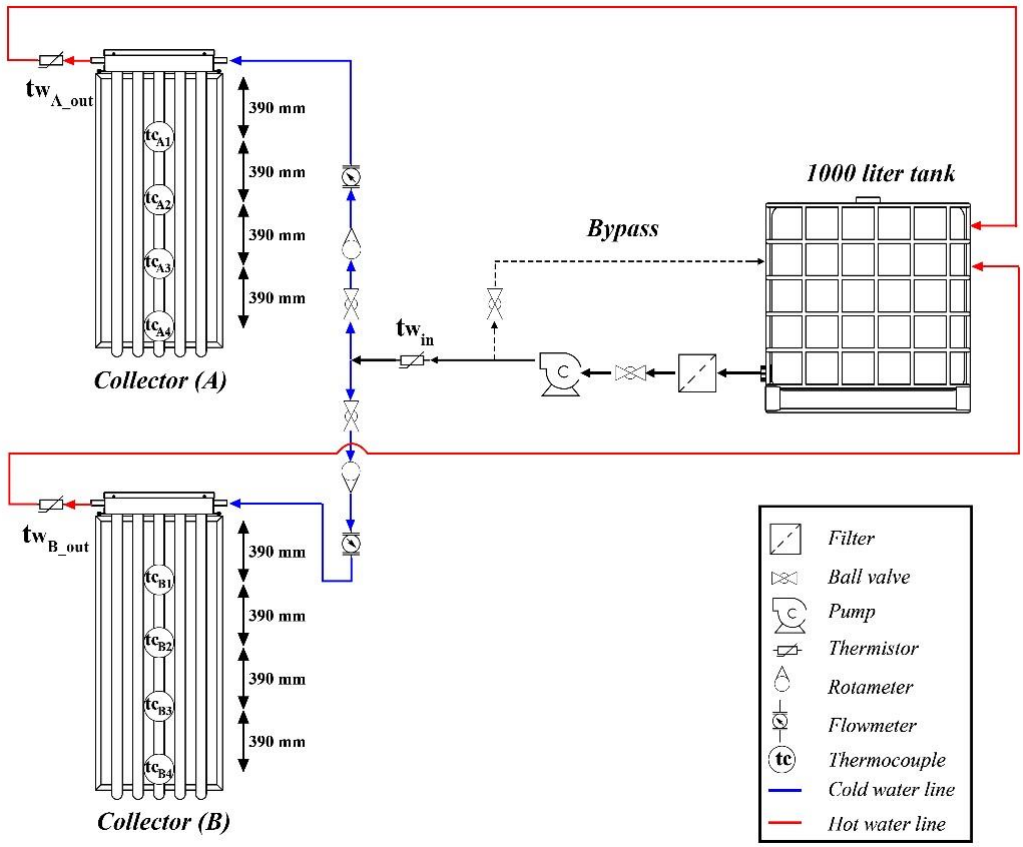

Figure 2. Schematic diagram for the experimental test rig

Figure 3. Photograph showing constructed test rig with two independent collectors

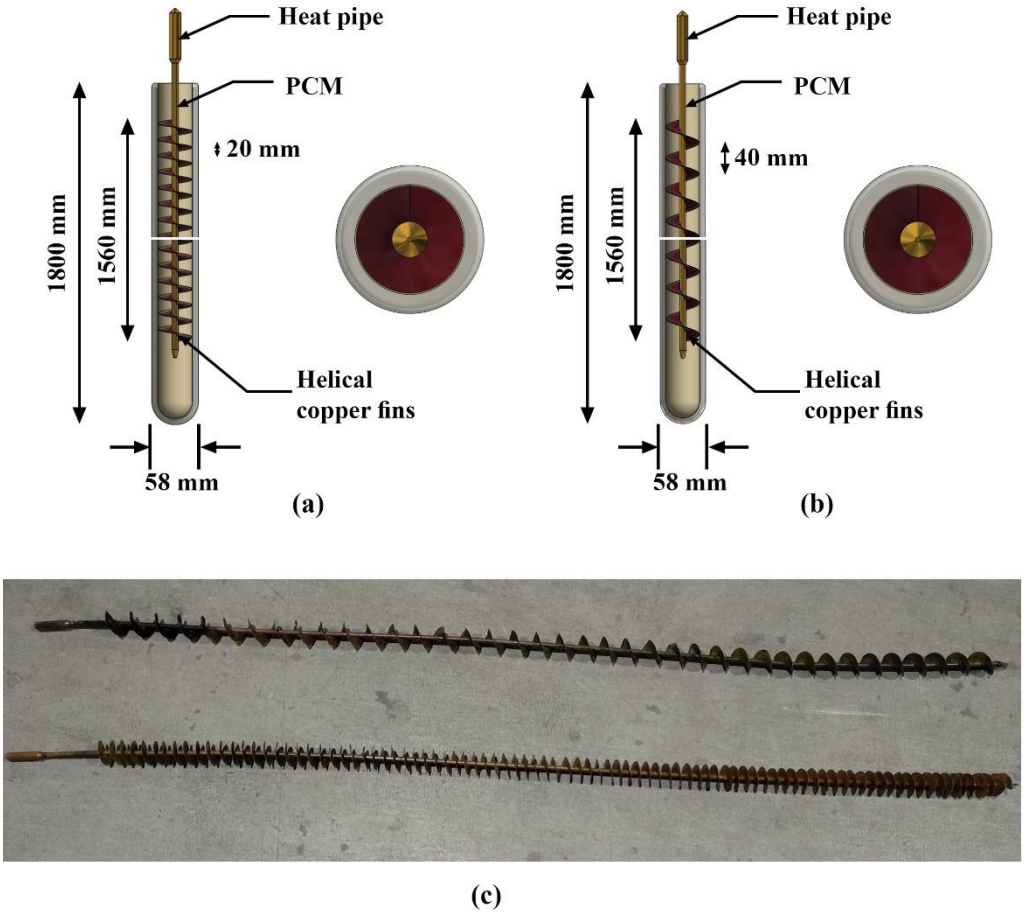

Figure 4. Sectional and top views for PCM integrated heat pipe ETSC: (a) Helical fins pitch 20, mm (b) Helical fins pitch 40, mm (c) Photo of two proposed helical fins systems

2.2. Experimental procedure and data reduction

The experimental test started while both collectors were covered. The pump is operated and the required flowrate was set. When stability had been achieved, the cover had been removed and data logging started. Global and diffused radiation intensities had been then measured and logged using a pyranometer every ten minutes until sunset. After sunset, the experiment had been kept running through the night till next morning sunrise. Data are still recorded and logged through that period. The amount of collected solar energy (Q_{coll}) by each collector was then calculated from the radiation data using the following equation:

$$Q_{coll} = \sum_{Sunrise}^{Sunset} I\, A_p\, \Delta\tau \qquad (1)$$

Where I is the global solar radiation intensity measured in W/m^2, A_p is the collector aperture area, and $\Delta\tau$ is the time step of logging the radiation data. A portion of this collected energy manifests in the rise of the HTF outlet temperature. Another portion is delivered to the PCM and causes temperature rise. The rest energy is wasted through losses. The ratio of these portions are shown to be dependent on the HTF flow rate.

The average daily efficiency (η_d) for each collector is the ratio between the useful energy (Q_{us}) delivered to the HTF causing a temperature rise and the value of the collected energy by the collector. Thus:

$$\eta_d = \frac{Q_{us}}{Q_{coll}} \qquad (2)$$

Q_{us} can be calculated by integrating the rate of useful energy transfer ($\dot{Q}_{us}$) as follows:

$$Q_{us} = \sum_{i=1}^{n} \dot{Q}_{us}\,\Delta\tau = \dot{m}\,C \sum_{i=1}^{n} (t_{out} - t_{in})\Delta\tau \qquad (3)$$

Where $\dot{m}$ is the HTF mass flow rate, C is the HTF specific heat, t_{out} and t_{in} are the HTF outlet and inlet temperatures respectively and $\Delta\tau$ is the time step at which the HTF temperature are measured and logged.

The performance of the two collectors was compared using enhancement ratio (ER). It's defined as the ratio between the differential useful energy delivered by each collector and the amount of useful energy delivered by the reference collector. The reference collector can be considered the collector which delivers less useful energy calculated through Equation 3. ER is expressed as:

$$ER = \frac{\left|Q_{us_B} - Q_{us_A}\right|}{Q_{us_{ref}}} \qquad (4)$$

The PCM temperature homogeneity achieved by each fins system can be expressed by the PCM temperature difference along the tube axis under peak PCM temperature conditions. This can be calculated using the following equations for both systems:

$$\Delta t_{(1,4)A} = tc_{A1} - tc_{A4} \qquad (5)$$

$$\Delta t_{(1,4)B} = tc_{B1} - tc_{B4} \qquad (6)$$

Definition of tc_{A1}, tc_{A4}, tc_{B1}, tc_{B4} are indicated in Figure 2.

2.3. Uncertainty analysis

2.3.1. Uncertainty of simple variables

Variables which can be measured directly through measuring equipment are defined as simple variables. These include; solar radiation intensity, HTF flowrate and HTF outlet and inlet temperatures. The uncertainty of these measuring equipment are summarized in Table 2.

Table 2 Uncertainty of simple variables

Variable	Uncertainty
Radiation intensity (I)	10 W/m^2
HTF flow rate (Q)	5%
HTF inlet and outlet temperatures (t_{out}, t_{in})	0.5 ˚C

2.3.2. Uncertainty of compound variables

Variables composed of more than one simple variable are defined as compound variables. The uncertainty for such variables can be calculated using Equation 7.

$$U_Y{}^2 = \left[\left(U_{x1}\frac{\partial Y}{\partial x_1}\right)^2 + \left(U_{x2}\frac{\partial Y}{\partial x_2}\right)^2 + \cdots + \left(U_{xn}\frac{\partial Y}{\partial x_n}\right)^2\right] \qquad (7)$$

The main compound variable investigated is the collector efficiency η. The uncertainty for the collector efficiency can be calculated using Equation 8:

$$\eta = \frac{useful\ energy}{collected\ energy} = \frac{\dot{m}\,C(t_{out} - t_{in})}{I\,A_p} = \frac{\rho\,C}{A_p}.\frac{Q(t_{out} - t_{in})}{I}\ \%\ (8)$$

If the flow is assumed to be incompressible, then the collector's efficiency becomes a function of four simple variables. These are; radiation intensity, HTF volumetric flow rate, HTF inlet temperature and HTF outlet temperature. Thus, the efficiency uncertainty can be calculated using Equation 7a;

$$U_\eta{}^2 = \left[\left(U_Q\frac{\partial \eta}{\partial Q}\right)^2 + \left(U_{t_{out}}\frac{\partial \eta}{t_{out}}\right)^2 + \left(U_{t_{in}}\frac{\partial \eta}{\partial t_{in}}\right)^2 + \left(U_I\frac{\partial \eta}{\partial I}\right)^2\right] \qquad (7a)$$

The differential of collector efficiency for the four simple variables can be calculate using the below Equations;

$$\frac{\partial \eta}{\partial Q} = \frac{\rho\, C}{A_p} \cdot \frac{(t_{out} - t_{in})}{I} \quad (9a)$$

$$\frac{\partial \eta}{\partial t_{out}} = \frac{\rho\, C}{A_p} \cdot \frac{Q}{I} \quad (9b)$$

$$\frac{\partial \eta}{\partial t_{in}} = -\frac{\rho\, C}{A_p} \cdot \frac{Q}{I} \quad (9c)$$

$$\frac{\partial \eta}{\partial I} = -\frac{\rho\, C}{A_p} \cdot \frac{Q(t_{out} - t_{in})}{I^2} \quad (9d)$$

Substituting in Equation 7a gives:

$$\therefore U_\eta{}^2 = \left[\left(U_Q \frac{\rho\, C}{A_p} \cdot \frac{(t_{out} - t_{in})}{I}\right)^2 + \left(U_{t_{out}} \frac{\rho\, C}{A_p} \cdot \frac{Q}{I}\right)^2 + \left(-U_{t_{in}} \frac{\rho\, C}{A_p} \cdot \frac{Q}{I}\right)^2 + \left(-U_I \frac{\rho\, C}{A_p} \cdot \frac{Q(t_{out} - t_{in})}{I^2}\right)^2\right] \quad (7b)$$

Performing a simple dimensional analysis shows that U_η is in fact dimensionless.
The collector's efficiency uncertainty can be calculated through Equation 7b for the four investigated flowrates. These results are presented in Table 3.

Table 3 Efficiency uncertainty for investigated flowrates

Test No.	Flow rate (L/min)	U_η
1	0.165	$1.11196*10^{-05}$
2	0.335	$1.59182*10^{-05}$
3	0.5	$2.1659*10^{-05}$
4	0.665	$2.61841*10^{-05}$

3. Results and discussion

Experimental tests were conducted at the period from August to October 2019. The solar collectors were tested under constant flowrate conditions. Selected days and considered HTF flow rates are given in Table 4.

Table 4 Experimental tests conditions

Test No.	Date	Flow rate (L/min)
1	October 8th 2019	0.165
2	September 25th 2019	0.335
3	September 1st 2019	0. 5
4	August 7th 2019	0.665

The variation of global solar radiation intensity and ambient temperature throughout the day is demonstrated in Figure 5 for predetermined days. It's worth noting that with the exception of short cloudy conditions, all test days were sunny.

3.1. PCM temperature variation

As the HTF flowrate increases, the portion of the collected thermal energy transferred to the fluid increases too. This in turn affects the amount of energy stored within the PCM.
From Figure 6, it is clear that at the smallest flow rate (0.165 L/min) the peak PCM temperatures obtained for systems A and B were 136.25 ˚C and 137 ˚C, respectively. This occurred at approximately 2:00 PM and indicates sunny weather condition at this hour as shown in the Figure 5a. However, it can be seen that system B demonstrated higher peak temperature compared to system A. The PCM temperature distribution for the two systems at 0.165 L/min flowrate is shown in Figure 6. The temperature of PCM at the end of the experiment for both system was between 40 ˚C and 50 ˚C indicating the system's ability to store energy throughout the day.

Figure 7 shows the PCM temperature distribution for both systems flow rate equals 0.335 L/min test conditions. It can be seen that the peak PCM temperatures were 130.5 ˚C and 129.5 ˚C for systems A and B, respectively. This occurred around 2:40 PM. The lower peak temperatures compared to that under 0.165 L/min conditions can be attributed to the cloudy weather conditions as well as the higher flow rate.

Figures 8&9 demonstrate PCM temperature distributions for both systems for 0.5 L/min and 0.665 L/min tests, respectively.

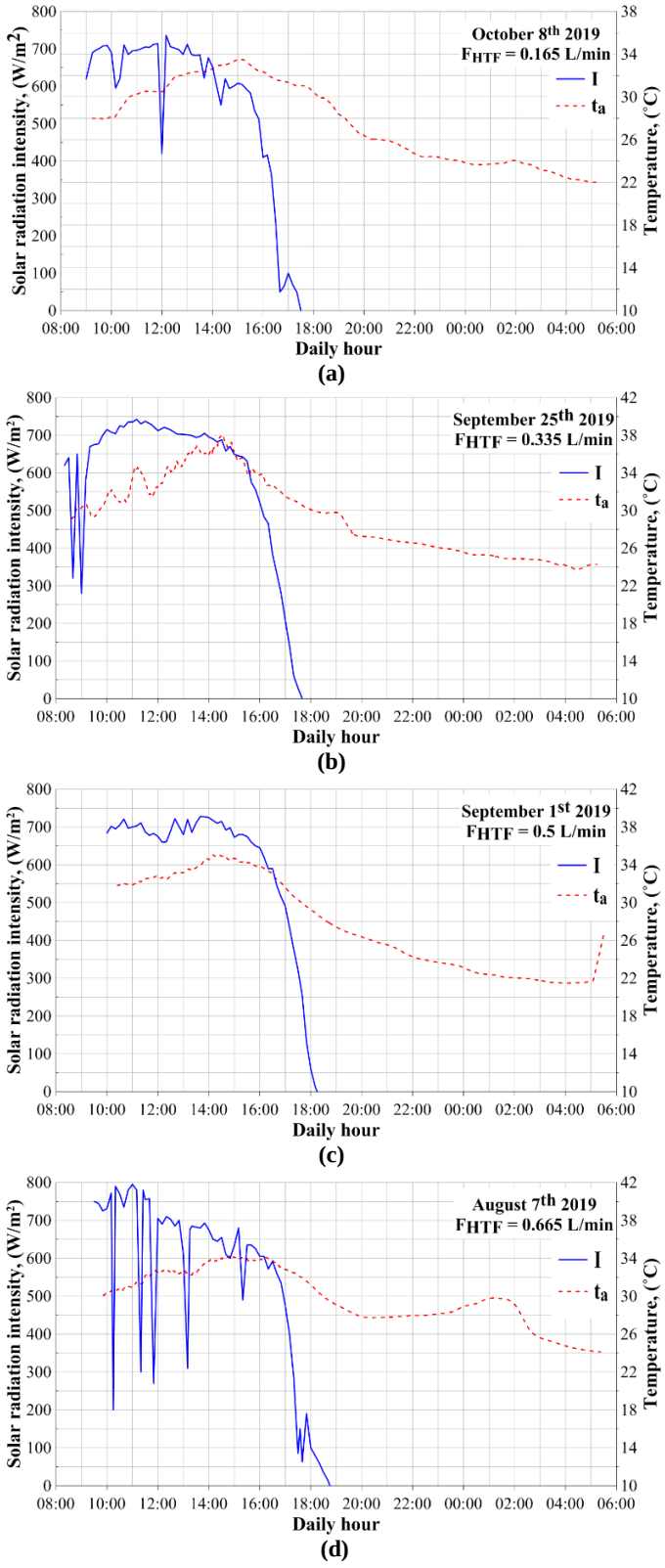

Fig. 5. Global inclined solar radiation I and Ambient Temperature t_a for the four test days, a, b, c and d

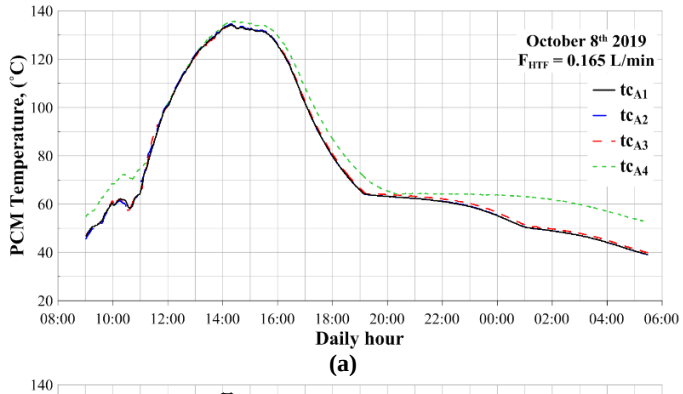

Figure 6. The PCM temperature variation of the 0.165 L/min flow rate for (a) system A with helical fins P = 20 mm, (b) System B with helical fins P = 40 mm

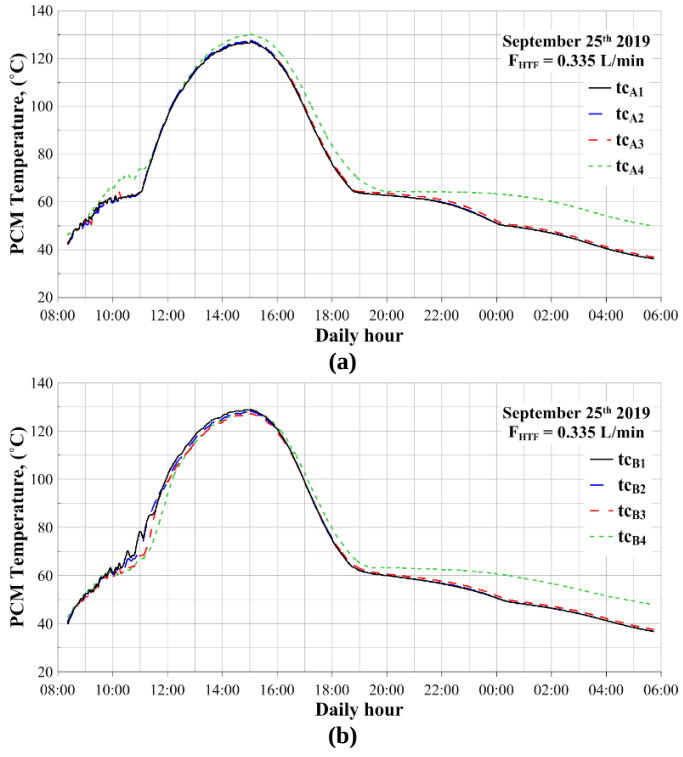

Figure 7. The PCM temperature variation of the 0.335 L/min flow rate for (a) system A with helical fins P = 20 mm, (b) System B with helical fins P = 40 mm

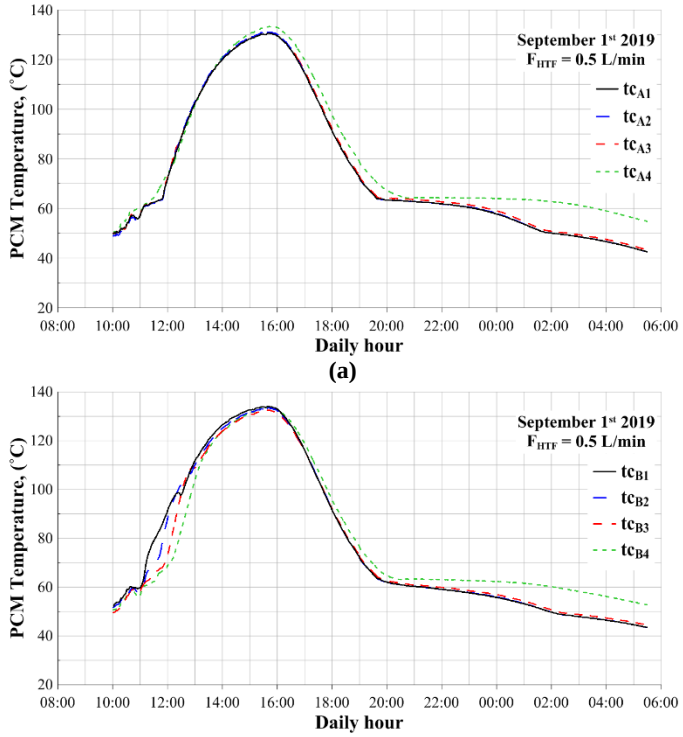

Figure 8. PCM temperature variation of the 0.5 L/min flow rate for (a) system A with helical fins P = 20 mm, (b) System B with helical fins P = 40 mm

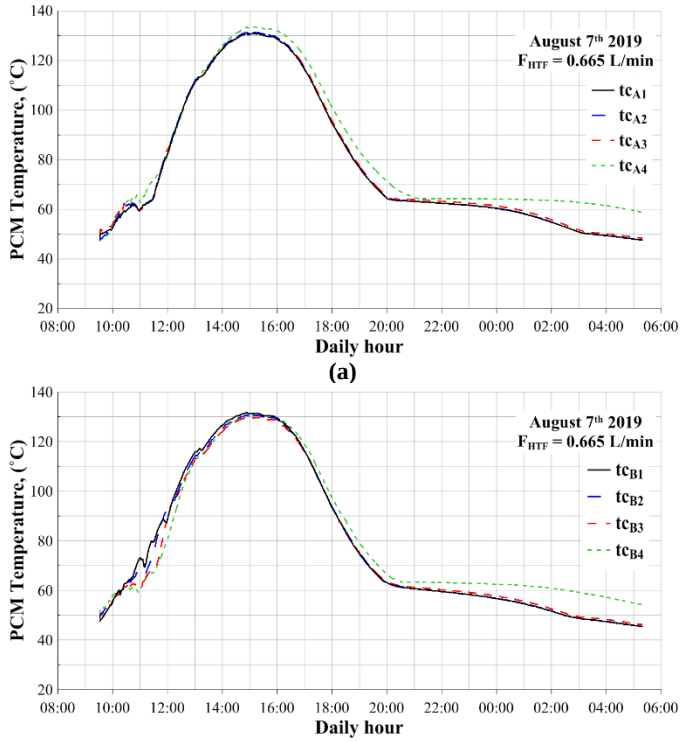

Figure 9. The PCM temperature variation of the 0.665 L/min flow rate for (a) system A with helical fins P = 20 mm, (b) System B with helical fins P = 40 mm

From Figures 6 through 9, it is noted that for system B having 40 mm fin pitch, during charging phase, the peak PCM temperature which was always recorded by thermocouple tc1 placed at the upper part of the evacuated tube, is affected by bouncy effect driving hot liquid PCM to the top of the evacuated tube and displacing the lower temperature PCM to the bottom. Consequently, the lowest PCM temperature at peak conditions were recorded by thermocouple tc4 located at near the bottom of the evacuated tubes. This also indicates that the proposed fins system with 40 mm pitch doesn't hinder bouncy flow.

Nevertheless, system A having 20 mm pitch fins, the maximum PCM peak temperature for charging phase was recorded by thermocouple tc4 while the lowest temperature was always recorded by thermocouple tc1. This reversed behaviour indicates that the smaller pitch slightly hindered the free flow buoyancy effect. Thus, trapping hot liquid PCM in the lower part of the evacuated tube. This can also be emphasized by the rapid transition from solid to liquid phase in the lower part of the evacuated tube for all four tested flowrates.

An important parameter for the fins systems performance is the temperature distribution homogeneity along the tube axis. This can be judged by the thermocouples temperature difference at peak conditions $\Delta t_{1-4}|_P$. Results show that both system provide a homogenous temperature distribution for the PCM. Maximum temperature difference at peak conditions of 3.5 were recorded for system B with 0.665 L/min test conditions. On the other hand, minimum peak temperature difference of 1.75 ˚C was recorded for system A with 0.165 L/min test conditions. The temperature difference at peak conditions for both systems A and B under the four tested flowrates are summarized in Table 5.

Table 5 PCM temperature difference at peak conditions

Flow rate (L/min)	$\Delta t_{1-4}\|_{P_A}$ (˚C)	$\Delta t_{1-4}\|_{P_B}$ (˚C)
0.165	1.75	3
0.335	3	3
0.5	3.25	2.75
0.665	3	3.5

During the discharge cycle, the sharp change of the PCM temperature slope in Figures 6 through 9 indicates the start of solidification. This phenomenon is due to the large amount of latent energy rejected at almost constant temperature. It can be observed that for both systems during the discharge cycle, the highest PCM temperature is recorded by tc4 near the evacuated tube bottom. Hence, the upper layers of PCM start solidification first. Thus, trapping the hot liquid PCM at the bottom of the evacuated tubes maintaining high temperature until the end of the test. Solidification starts at the top layers. This is because the top layers are closer to the evacuated tube opening which causes energy losses to the surrounding. Moreover, the heat pipe liquid condensate passes through the upper layers first absorbing heat as it flows down past the bottom layers. This discharge process is also emphasized by the slower temperature deterioration of tc4 from the start of solidification till the end of the experiment.

The main function of PCM is to store energy and prolong the period of useful energy availability. It's interesting to compare the liquid to solid phase change starting hour indicated as LSPC_H for both systems. To further gain a clearer picture, this time can also be compared to the sunset hour for the test day. Results shows that the maximum delay of the start of solidification was 1 hour and 43 minutes from sunset for system B under 0.5 L/min test conditions. On the other hand, the minimum delay of start of solidification was 1 hour and 12 minutes from sunset for both systems under 0.335 L/min test condition. Time of solidification of the liquid PCM for both systems under the four tested flowrates are summarized in Table 6.

Table 6 Start time of PCM's liquid to solid phase change

Flow rate (L/min)	LSPC_H$_A$	LSPC_H$_B$	Sunset hour
0.165	7:15 pm	7:15 pm	5:30 pm
0.335	7:00 pm	7:00 pm	5:48 pm
0.5	7:45 pm	8:00 pm	6:17 pm
0.665	8:00 pm	8:00 pm	6:44 pm

3.2. HTF outlet temperature

One of the most dominant effect to uses solar collectors can be detected analysing the inlet-outlet temperatures of HTF throughout the day.

Figure 10 shows the HTF inlet and outlet temperatures distribution throughout the day for the four tested flowrates. It can be observed that there is a trend for increasing the peak HTF outlet temperature with decreasing HTF flowrate. This is because lower flowrates require less amount of useful energy for its temperature rise.

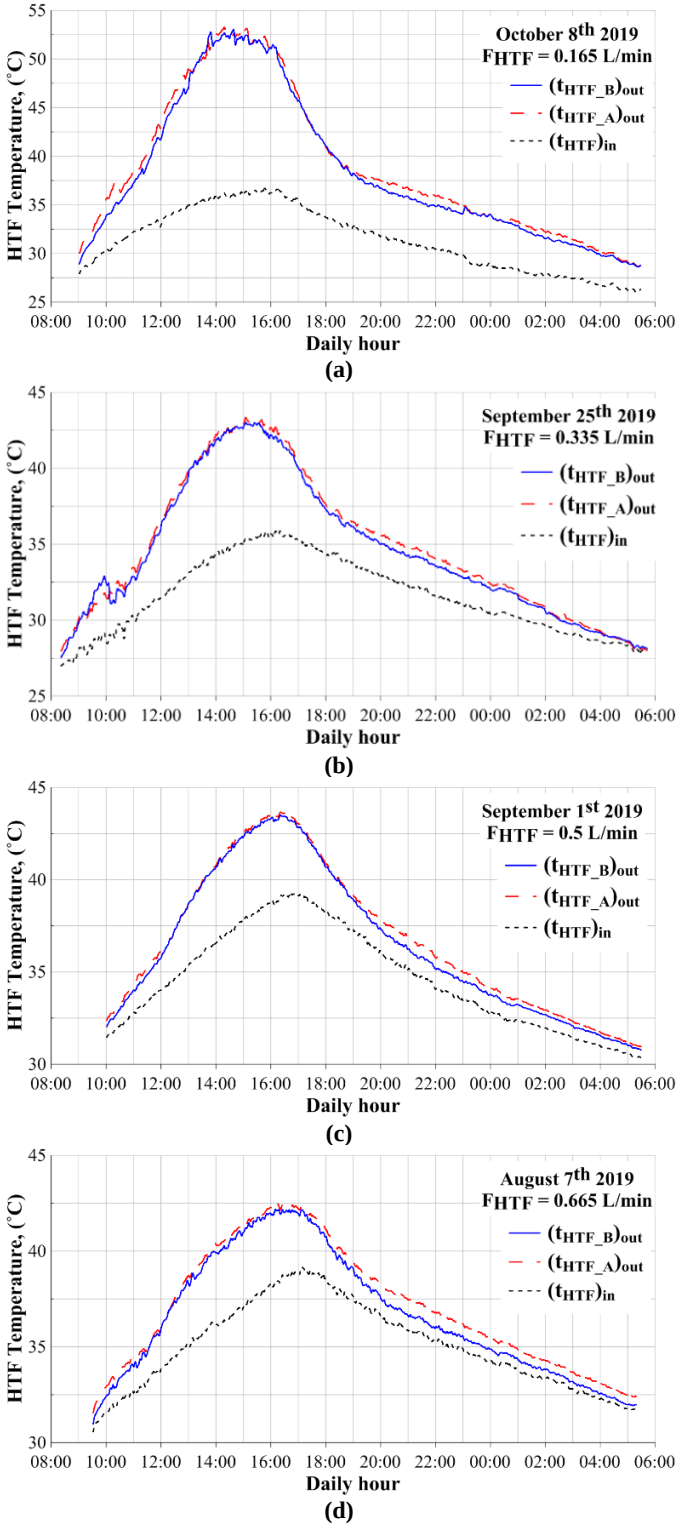

Fig. 10. HTF inlet and outlet temperatures for both collectors A & B for (a) 0.165 L/min (b)0.335 L/min (c) 0.5 L/min (d) 0.665 L/min

The maximum peak HTF outlet temperature occurred for system A under 0.165 L/min test conditions and was equal to 53.6 ˚C. At peak conditions, the HTF inlet temperature was 35.3 ˚C. This resulted in HTF temperature rise of about 18.3 ˚C. For the same conditions, the peak HTF outlet temperature for collector B was 53.25 ˚C. On the other hand, the lowest peak HTF outlet temperature was recorded for system B under 0.665 L/min test conditions and was equal to 42.3 ˚C. For the same conditions, the HTF inlet temperature was 38.5 ˚C. Hence, the temperature rise is 3.9 ˚C. Under the same test conditions, the peak HTF outlet temperature for system A was 42.5 ˚C. The peak HTF outlet temperature as well as the corresponding inlet temperature are summarized in Table 7. It should also be noted that for both systems, the peak outlet HTF temperature occurred at noon where the PCM temperature was near maximum. It's also noticed that system A had a slightly higher peak HTF outlet temperature than that of system B for all tested flow rates.

Table 7 Inlet and outlet peak HTF temperatures and corresponding temperature differences

Flow rate (L/min)	$_{HTF}\|_{P_{in}}$ (˚C)	$_{HTF}\|_{P_A}$ (˚C)	$t_{HTF}\|_A$ (˚C)	$_{HTF}\|_{P_B}$ (˚C)	$\Delta t_{HTF}\|_B$ (˚C)
0.165	35.3	53.6	18.3	53.25	17.95
0.335	35.4	43.45	8.05	43.1	7.7
0.5	38.9	43.7	4.8	43.5	4.6
0.665	38.5	42.5	4	42.3	3.8

During the discharge phase where solar radiation is scarce or absent, it can be seen that PCM temperature inside the evacuated tubes start declining. This indicates that the energy stored within PCM is being discharged to keep HTF outlet at elevated temperatures. Results show that PCM integration and the use of helical fins keep the HTF outlet temperature higher than the inlet throughout the discharge phase for all tested flowrates. This emphasis the advantages of utilizing a latent heat storage system coupled with an efficient fins system in prolonging the period of useful energy availability. It can also be observed that HTF outlet temperature for system A is higher than that of system B through the discharge cycle for all flowrates. This indicates better energy utilization for the fins system with 20 mm pitch.

3.3. Effect of flow rate on the systems daily efficiency and enhancement ratio

The daily efficiency for considered conditions predicted by equation (2) are listed in Table 8. Enhancement ratio (ER) delivered by one fin system over the other is calculated as per equation (4).

Table 8 System efficiency and enhancement ratio for the four tested flow rates

Flow rate (L/min)	η_{d_A}	η_{d_B}	ER
0.165	63.50%	60.56%	4.9%
0.335	60.78%	57.00%	6.63%
0.5	66.00%	61.27%	7.72%
0.665	68.66%	61.39%	11.85%

From the above results, it could be seen that the system daily efficiency for system A was higher than that of system B for all tested flowrates. It is also noted that the maximum enhancement ratio of system A was about 11.85% for 0.665 L/min test conditions. On the other hand, the minimum enhancement ratio for system A was about 4.9% for 0.165 L/min test conditions. This could be explained by noting that lower flowrates are accompanied by higher temperatures. This in turn, encourages convection losses. Moreover, at lower flowrates, the PCM solidification process becomes slow. This causes formation of solid PCM layer on the helical fins surface which hinders convection heat transfer to the heat pipe. On the other hand, higher flowrates are accompanied by lower temperature differences which reduces energy losses through convection.

These results could be compared to other ETSCs modifications techniques. Dan Nchelatebe Nkwetta et al. [19] proposed a modification based on ETSC system integrated with single sided parabolic concentrator. Results have shown that the single sided concentrator provided up to 25.42% increase in the daily collected energy compared to a control collector.

4. Conclusions

The thermal performance of a heat pipe ETSC integrated with PCM had been investigated experimentally. The study considered two novel helical fins with different pitches under four different thermal loads. The findings of the present work are drawn as follows:

1- Both helical fins systems provide good thermal transfer to the PCM. This is indicated by the PCM temperature distribution homogeneity along the tube axis. Minimum temperature difference along the tube axis about 1.75 ˚C which was achieved by System A. While largest difference about 3.5 ˚C and achieved by system B.
2- The smaller helical pitch hindered the free buoyancy flow of the PCM inside the tube. This is indicated by the higher bottom temperature through the charge and discharge process.
3- Both finned tubes systems delivered enough thermal energy to PCM to delay the start of the solidification by a maximum of one hour and forty-five minutes from sunset.
4- Both finned tubes systems prolonged the period of availability of useful energy for all four tested flowrates. This is shown in HTF outlet temperature which was kept higher than the inlet temperature throughout the day for all tested flowrates. The peak HTF outlet temperature was 53.6 ˚C which was achieved by system A under 0.165 L/min test conditions.
5- For all four flowrates, system A provided a higher daily efficiency than that of system B. The maximum efficiency was about 68.66 % achieved by system A with an enhancement ratio of about 11.85%.

Nomenclature

A_p	Collector aperture area, (W/m^2)
C	Specific heat, (J/kg.K)
ER	Enhancement ratio
I	Instantaneous solar radiation intensity, (W/m^2)
F	Working fluid flowrate, (L/min)
$\dot{m}$	Working fluid mass flowrate, (kg/s)
Q_{coll}	Collected daily solar energy, (MJ)
Q_{us}	Collector's useful energy, (MJ)
$\dot{Q}_{us}$	Collector's rate of useful energy, (MW)
t	Temperature, (˚C)

Greek symbols

η_d	System daily efficiency
τ	Time, (s)
Δ	Difference

Subscripts

A	Collector A
a	Ambient air
B	Collector B
In	Inlet to collector
Out	Outlet from collector
P	Peak condition
Sunrise	Time of sunrise
Sunset	Time of sunset

Abbreviations

CPC	Compound parabolic concentrator
CNT	Carbon Nanotube
ETSC	Evacuated tube solar collector
HTF	Heat transfer fluid
LSPC_H	Liquid to solid phase change starting hour
NCPCM	Nanocomposite phase changing material
PCM	Phase changing material
tc	Thermocouple
TES	Thermal energy storage

References

[1] Sharma SD, Iwata T, Kitano H, Sagara K. Thermal performance of a solar cooker based on an evacuated tube solar collector with a PCM storage unit. Sol Energy 2005;78:416–26. doi:https://doi.org/10.1016/j.solener.2004.08.001.

[2] Naghavi MS, Ong KS, Badruddin IA, Mehrali M, Silakhori M, Metselaar HSC. Theoretical model of an evacuated tube heat pipe solar collector integrated with phase change material. Energy 2015;91:911–24. doi:10.1016/j.energy.2015.08.100.

[3] Mehla N, Yadav A. Experimental analysis of thermal performance of evacuated tube solar air collector with phase change material for sunshine and off-sunshine hours. Int J Ambient Energy 2017;38:130–45. doi:10.1080/01430750.2015.1074612.

[4] Mehla N, Yadav A. Thermal analysis on charging and discharging behaviour of a phase change material-based evacuated tube solar air collector. Indoor Built Environ 2018;27:156–72. doi:10.1177/1420326X16667626.

[5] Mehla N, Yadav A. Experimental investigation of a desiccant dehumidifier based on evacuated tube solar collector with a PCM storage unit. Dry Technol 2017;35:417–32. doi:10.1080/07373937.2016.1180300.

[6] Bai Y, He X, Liu Y, Duan J, Wang Y, Han X. Experimental investigation of a solar thermal storage heater assembled with finned heat pipe and collective vacuum tubes. Energy Convers Manag 2018;166:463–73. doi:10.1016/j.enconman.2018.04.034.

[7] Xue HS. Experimental investigation of a domestic solar water heater with solar collector coupled phase-change energy storage. Renew Energy 2016;86:257–61. doi:10.1016/j.renene.2015.08.017.

[8] Essa MA, Mostafa NH, Ibrahim MM. An experimental investigation of the phase change process e ff ects on the system performance for the evacuated tube solar collectors integrated with PCMs. Energy Convers Manag 2018;177:1–10. doi:10.1016/j.enconman.2018.09.045.

[9] Abokersh MH, El-Morsi M, Sharaf O, Abdelrahman W. On-demand operation of a compact solar water heater based on U-pipe evacuated tube solar collector combined with phase change material. Sol Energy 2017;155:1130–47. doi:10.1016/j.solener.2017.07.008.

[10] Feliński P, Sekret R. Experimental study of evacuated tube collector/storage system containing paraffin as a PCM. Energy 2016;114:1063–72. doi:10.1016/j.energy.2016.08.057.

[11] Feliński P, Sekret R. Effect of PCM application inside an evacuated tube collector on the thermal performance of a domestic hot water system. Energy Build 2017;152:558–67. doi:10.1016/j.enbuild.2017.07.065.

[12] Feliński P, Sekret R. Effect of a low cost parabolic reflector on the charging efficiency of an evacuated tube collector/storage system with a PCM. Sol Energy 2017;144:758–66. doi:10.1016/j.solener.2017.01.073.

[13] Papadimitratos A, Sobhansarbandi S, Pozdin V, Zakhidov A, Hassanipour F. Evacuated tube solar collectors integrated with phase change materials. Sol Energy 2016;129:10–9. doi:10.1016/j.solener.2015.12.040.

[14] Naghavi MS, Ong KS, Badruddin IA, Mehrali M, Metselaar HSC. Thermal performance of a compact design heat pipe solar collector with latent heat storage in charging/discharging modes. Energy 2017;127:101–15. doi:10.1016/j.energy.2017.03.097.

[15] Sobhansarbandi S, Martinez PM, Papadimitratos A, Zakhidov A, Hassanipour F. Evacuated tube solar collector with multifunctional absorber layers. Sol Energy 2017;146:342–50. doi:10.1016/j.solener.2017.02.038.

[16] Li B, Zhai X. Experimental investigation and theoretical analysis on a mid-temperature solar collector/storage system with composite PCM. Appl Therm Eng 2017;124:34–43. doi:10.1016/j.applthermaleng.2017.06.002.

[17] Li B, Zhai X, Cheng X. Experimental and numerical investigation of a solar collector/storage system with composite phase change materials. Sol Energy 2018;164:65–76. doi:10.1016/j.solener.2018.02.031.

[18] Manoj Kumar P, Mylsamy K. Experimental investigation of solar water heater integrated with a nanocomposite phase change material: Energetic and exergetic approach. J Therm Anal Calorim 2019;136:121–32. doi:10.1007/s10973-018-7937-9.

[19] Nkwetta DN, Smyth M, Zacharopoulos A, Hyde T. In-door experimental analysis of concentrated and non-concentrated evacuated tube heat pipe collectors for medium temperature applications. Energy Build 2012;47:674 81.doi:10.1016/j.enbuild.2012.01.010.